Crystal Structure and Sodium Environments in Sodium Tetratellurite, $Na_2Te_4O_9$, and Sodium Tellurite, Na_2TeO_3, by X-ray Crystallography and Sodium-23 NMR

S. L. Tagg, J. C. Huffman, and J. W. Zwanziger*

Department of Chemistry and Molecular Structure Center, Indiana University, Bloomington, Indiana 47405

Received May 20, 1994. Revised Manuscript Received July 25, 1994[⊗]

We report the results of structural studies on two of the crystalline phases in the sodium tellurite family, $(Na_2O)_x(TeO_2)_{1-x}$. Our primary result is the first X-ray crystallographic structure determination of the $x = 0.20$ phase, $Na_2Te_4O_9$ ($P\bar{1}$, $a = 7.336(1)$ Å, $b = 10.449(1)$ Å, $c = 6.876(1)$ Å, $\alpha = 90.11(1)°$, $\beta = 110.95(1)°$, $\gamma = 69.52(1)°$, $V = 456.48$ Å^3, $Z = 2$). The structure of this compound is intermediate between that of the $x = 0.0$ (TeO_2) and $x = 0.50$ (Na_2TeO_3) phases, in that it exhibits both bridging and nonbridging oxygen. We have also studied the sodium cation binding interaction through solid-state NMR in the $Na_2Te_4O_9$ and Na_2TeO_3 phases, using magic-angle, variable-angle, and dynamic-angle spinning techniques. We have measured the chemical shifts and quadrupole interaction parameters of the different sodium sites, which we correlate with the crystal structures.

Introduction

Tellurite glasses possess useful properties including low melting temperatures, high refractive indexes, and high transmission in the infrared region. These TeO_2-based materials are also resistant to devitrification, and their applicability, unlike the hygroscopic phosphate and borate analogs, is not limited by chemical instability with respect to water. Modification of tellurite by alkali oxides, M_2O, produces $(M_2O)_x(TeO_2)_{1-x}$ glasses over a broad range of x, although pure TeO_2 itself is only a conditional glass-former. Using sodium oxide as the modifier leads to a particularly interesting glass-forming system, characterized by especially stable glasses in the composition region near $x = 0.20$. This stability is surprising, because this system is also known to exhibit a crystalline phase at $x = 0.20$ ($Na_2Te_4O_9$), in addition to others at $x = 0.0$ (TeO_2), $x = 0.33$ ($Na_2Te_2O_5$), and $x = 0.50$ (Na_2TeO_3).[1] One typically expects glass stability at eutectic compositions, not at crystal phases. The glasses have been studied with a variety of structural probes including IR,[2] Raman,[2,3] and Mössbauer[4] spectroscopies, as well as by thermal methods including DSC[2,5] and DTA.[4] In the crystals, previously only the structures of TeO_2[6,7] and Na_2TeO_3[8] had been determined. The structures of $Na_2Te_4O_9$ and $Na_2Te_2O_5$ are of interest, both in their own right and as aids in interpreting studies of the glass structure. The purpose of the present paper is to report the structure of $Na_2Te_4O_9$ as determined by X-ray crystallography. We also report detailed NMR measurements of the sodium cation binding in both $Na_2Te_4O_9$ and Na_2TeO_3.

Experimental Methods

Sample Preparation. $Na_2Te_4O_9$ was prepared from stoichiometric amounts of tellurium(IV) oxide (TeO_2, 99.995%, Aldrich) and sodium carbonate (99.995+%, Aldrich). The mixture (3–4 g) was placed in a silica glass tube, heated at 750 °C for approximately 8 min, and then poured onto a stainless steel plate. Pieces of the resulting colorless glass were then placed in a silica glass boat and annealed at 460 °C, 10 °C below the reported melting temperature.[9] After 24 h, the furnace was set to room temperature and allowed to cool (approximately 2 °C/min). Colorless, platelike crystals were produced.

The studies of Na_2TeO_3 were performed on a commercial sample (Cerac, Inc.) with no further purification.

X-ray Structure Determination of $Na_2Te_4O_9$. Colorless crystals of $Na_2Te_4O_9$ were obtained from the melt, as described above. A small crystal fragment was cleaved from a larger sample and affixed to the end of a glass fiber using silicone grease, and the mounted sample was then transferred to the goniostat where it was cooled to −171 °C for characterization and data collection. A systematic search of a limited hemisphere of reciprocal space located a set of reflections with no symmetry or systematic absences, indicating a triclinic space group. Subsequent solution and refinement of the structure confirmed $P\bar{1}$ to be the proper space group (Table 1).

Data were collected using a standard moving crystal, moving detector technique with fixed background counts at each extreme of the scan. Data were corrected for Lorentz and polarization terms and equivalent data averaged after correction for absorption. The structure was solved by direct methods (SHELXS-86) and Fourier techniques. A final difference Fourier was essentially featureless, the largest peak being 0.54 e/Å^3. The single-phase character of the sample of $Na_2Te_4O_9$ was verified by checking that the X-ray powder pattern computed from the determined structure matched the powder pattern obtained experimentally from the bulk sample.

[⊗] Abstract published in *Advance ACS Abstracts,* September 1, 1994.

(1) Hantke, G., Ed. *Tellur. Gmelin Handbuch der Anorganischen Chemie*; Springer-Verlag: Berlin, 1976.
(2) Heo, J.; Lam, D.; Sigel, Jr., G. H.; Mendoza, E. A.; Hensley, D. A. *J. Am. Ceram. Soc.* **1992**, *75*, 227.
(3) Sekiya, T.; Mochida, N.; Ohtsuka, A.; Tonokawa, M. *J. Non-Cryst. Solids* **1992**, *144*, 128.
(4) Nishida, T.; Saruwatari, S.; Takashima, Y. *Bull. Chem. Soc. Jpn.* **1988**, *61*, 4093.
(5) Zhang, M.; Mancini, S.; Bresser, W.; Boolchand, P. *J. Non-Cryst. Solids* **1992**, *151*, 149.
(6) Lindqvist, O. *Acta Chem. Scand.* **1968**, *22*, 977.
(7) Beyer, H. *Z. Kristallogr.* **1967**, *124*, 228.
(8) Masse, R.; Guitel, J. C.; Tordjman, I. *Mater. Res. Bull.* **1980**, *15*, 431.
(9) Khachaturyan, T. A.; Samplavskaya, K. K.; Karapet'yants, M. K. *Russ. J. Inorg. Chem.* **1970**, *15*, 1759.

0897-4756/94/2806-1884$04.50/0

Table 1. Crystallographic Data on $Na_2Te_4O_9$

molar mass	700.37		
Crystal Data			
crystal system	triclinic	space group	$P\bar{1}$
a, Å	7.336(1)	α, deg	90.11(1)
b, Å	10.449(1)	β, deg	110.95(1)
c, Å	6.876(1)	γ, deg	69.52(1)
V, Å^3	456.48	Z (molecules/cell)	2
ϱ_{calcd}, g cm^{-3}	5.096	linear abs coeff, cm^{-1}	128.146
Data Collection			
T, °C	−171	Mo Kα λ, Å	0.710 69
2θ min, max/deg	6, 55	obsd data $I > 2.33\sigma(I)$	2064
Refinement			
no. of params	137	goodness of fit	4.775
$\Delta\varrho$(max), e/Å^3	0.54	R	0.0426
R_w	0.0541	R_{merge}	0.020

Characterization by NMR. NMR spectra of sodium-23 in $Na_2Te_4O_9$ and Na_2TeO_3 were obtained using a home-built spectrometer using both a 4.7 T magnet and an 8.46 T magnet. The Larmor frequencies of ^{23}Na in these fields are 52.9 and 95.2 MHz, respectively. In both cases a commercial switched angle sample spinning NMR probe (Doty Scientific) was used. A variety of experiments were employed, including magic-angle spinning (MAS), variable-angle spinning (VAS), and dynamic-angle spinning (DAS). In all cases the sample was spun at frequencies near 7 kHz. The relaxation times in the samples were determined with saturation−recovery experiments and found to be about 8 s for both sites in both samples. Signal-averaging in all the NMR experiments was therefore performed with delays of 50 s between scans.

The MAS and VAS experiments were performed both as pulse−acquire experiments and with acquisition following formation of a Hahn echo (pulse sequence $\pi/2_x-\tau-\pi_y$), to minimize spectrometer dead-time problems. Typically 500−800 scans were averaged for each spectrum. Because of the quadrupole interaction to which the sodium-23 nuclei are subject, these experiments do not fully resolve the cation sites in these materials. Therefore we also used dynamic-angle spinning (DAS) NMR.[10,11] In contrast to MAS and VAS, the DAS experiment is a two-dimensional "separation of interactions" experiment.[12] DAS yields a spectrum in which one axis reflects only the isotropic shift (chemical shift plus second-order quadrupole shift), and the other shows anisotropic shift contributions as well. The result is a high-resolution spectrum and additionally powder patterns for each site with no spectral overlap. The shifted-echo DAS sequence of Grandinetti et al. was used,[11] in which the full DAS echo is acquired, in order to obtain purely absorptive phase two-dimensional spectra. For this experiment 64 scans were averaged at each increment in the t_1 time domain.

Results

Experimental details of the crystallography are given in Table 1. Fractional coordinates of $Na_2Te_4O_9$ are given in Table 2, and selected bond lengths and angles in Tables 3 and 4. The unit cell of $Na_2Te_4O_9$ is pictured in Figure 1.

Figure 2 shows representative ^{23}Na NMR spectra of $Na_2Te_4O_9$, with the sample spinning rapidly about an axis inclined at different angles with respect to the magnetic field. These angles include the usual magic angle (54.74°), and a fourth-rank magic angle (70.12°). The reasons for choosing these angles are discussed below. Figure 3 shows a representative two-dimen-

Table 2. Fractional Coordinates and Equivalent Isotropic Thermal Parameters B_{iso} for $Na_2Te_4O_9$[a]

atom	x	y	z	B_{iso} (Å^2)
Te(1)	0.2825(1)	0.0128(1)	0.0109(1)	0.53(2)
Te(2)	0.6380(1)	0.2114(1)	−0.5416(1)	0.56(2)
Te(3)	0.2051(1)	0.1931(1)	0.5169(1)	0.57(2)
Te(4)	0.3254(1)	0.6715(1)	0.0272(1)	0.57(2)
Na(5)	0.2223(7)	0.5110(4)	−0.5239(6)	1.01(7)
Na(6)	0.1800(6)	0.3633(4)	−1.0224(6)	0.81(6)
O(7)	0.4941(12)	−0.1068(7)	0.3302(11)	0.89(11)
O(8)	0.3416(11)	0.2967(8)	−0.6641(11)	0.91(11)
O(9)	0.3070(12)	0.6728(8)	0.7120(11)	1.00(11)
O(10)	0.1441(11)	0.3524(7)	0.6320(11)	0.80(11)
O(11)	0.4997(11)	0.1150(7)	0.0581(11)	0.71(10)
O(12)	0.3312(12)	0.6661(8)	0.3375(10)	0.86(11)
O(13)	0.1351(11)	0.0929(7)	0.7129(10)	0.72(10)
O(14)	0.8764(11)	0.4027(7)	0.0415(11)	0.85(11)
O(15)	0.1559(11)	0.8630(7)	0.9699(11)	0.91(11)

[a] $B_{iso} = (8\pi^2/3)\sum_i U_{ii}$, where the U_{ii} are the diagonal elements of the anisotropic thermal parameters.[28,29]

Table 3. Selected Bond Lengths in $Na_2Te_4O_9$

bond	dist (Å)	bond	dist (Å)
Te(1)−Te(1[a])	3.1653(13)	Te(1)−Te(4[b])	3.4673(10)
Te(1)−Te(3[c])	3.6481(10)	Te(1)−Te(3[d])	3.8652(11)
Te(1)−O(11[a])	1.899(7)	Te(1)−O(13[c])	1.964(7)
Te(1)−O(15[e])	2.055(7)	Te(1)−O(11)	2.146(7)
Te(1)−O(7)	2.238(7)		
Te(2)−O(8)	1.889(7)	Te(2)−O(12[f])	1.905(7)
Te(2)−O(9[f])	1.920(7)	Te(2)−O(7[a])	2.450(7)
Te(3)−O(10)	1.823(7)	Te(3)−O(7[d])	1.934(7)
Te(3)−O(13)	2.014(6)	Te(3)−O(8[g])	2.320(7)
Te(4)−O(14[f])	1.822(7)	Te(4)−O(15[c])	1.902(7)
Te(4)−O(12)	2.119(7)	Te(4)−O(9[c])	2.122(7)
Na(5)−Na(5[k])	3.476(8)	Na(5)−Na(6[i])	3.299(6)
Na(5)−O(10[c])	2.310(8)	Na(5)−O(12[c])	2.373(8)
Na(5)−O(10[j])	2.388(8)	Na(5)−O(9)	2.424(8)
Na(5)−O(8)	2.436(8)	Na(5)−O(12[f])	2.926(9)
Na(6)−Na(6[i])	3.244(8)		
Na(6)−O(8)	2.302(8)	Na(6)−O(10[k])	2.303(8)
Na(6)−O(14[l])	2.319(8)	Na(6)−O(14[m])	2.328(8)
Na(6)−O(11[c])	2.713(8)		

[a] $\bar{x}+1, \bar{y}, \bar{z}$. [b] $x, y-1, z$. [c] $x, y, z-1$. [d] $\bar{x}+1, \bar{y}, \bar{z}+1$. [e] $x, y-1, z-1$. [f] $\bar{x}+1, \bar{y}+1, \bar{z}$. [g] $x, y, z+1$. [h] $\bar{x}, \bar{y}+1, \bar{z}-1$. [i] $\bar{x}, \bar{y}+1, \bar{z}-2$. [j] $\bar{x}, \bar{y}+1, \bar{z}$. [k] $x, y, z-2$. [l] $x-1, y, z-1$. [m] $\bar{x}+1, \bar{y}+1, \bar{z}-1$.

Table 4. Selected Bond Angles in $Na_2Te_4O_9$

bond	angle (deg)	bond	angle (deg)
O(11[a])−Te(1)−O(13[b])	88.7(3)	O(11)−Te(1)−O(7)	86.43(26)
O(11[a])−Te(1)−O(15[c])	85.6(3)	O(11[a])−Te(1)−O(11)	77.2(3)
O(11[a])−Te(1)−O(7)	80.55(28)	O(13[b])−Te(1)−O(15[c])	92.9(3)
O(13[b])−Te(1)−O(11)	91.85(27)	O(13[b])−Te(1)−O(7)	169.26(27)
O(15[c])−Te(1)−O(11)	162.00(28)	O(15[c])−Te(1)−O(7)	85.71(28)
O(10)−Te(3)−O(7[d])	101.3(3)	O(13)−Te(3)−O(8[e])	170.33(26)
O(10)−Te(3)−O(13)	93.5(3)	O(10)−Te(3)−O(8[e])	85.91(27)
O(7[d])−Te(3)−O(13)	94.2(3)	O(7[d])−Te(3)−O(8[e])	76.51(28)
O(10[b])−Na(5)−O(12[f])	89.58(27)	O(10[b])−Na(5)−O(12[b])	175(5)
O(10[b])−Na(5)−O(10[g])	84.6(3)	O(10[b])−Na(5)−O(9[b])	111.2(4)
O(10[b])−Na(5)−O(8)	73.6(4)	O(12[f])−Na(5)−O(12[b])	86.0(3)
O(12[f])−Na(5)−O(10[g])	172(3)	O(12[f])−Na(5)−O(9[b])	87.27(26)
O(12[f])−Na(5)−O(8)	61.8(3)	O(12[b])−Na(5)−O(10[g])	99.6(3)
O(12[b])−Na(5)−O(9[b])	66.9(4)	O(12[b])−Na(5)−O(8)	105.7(4)
O(10[h])−Na(6)−O(14[i])	94.5(3)	O(10[h])−Na(6)−O(14[j])	115.5(4)
O(10[h])−Na(6)−O(8)	156(1)	O(10[h])−Na(6)−O(11[b])	85.02(27)
O(14[i])−Na(6)−O(14[j])	91.5(3)	O(14[i])−Na(6)−O(8)	100.7(3)
O(14[i])−Na(6)−O(11[b])	139.7(5)	O(14[j])−Na(6)−O(8)	83.1(3)
O(14[j])−Na(6)−O(11[b])	125.1(4)		

[a] $\bar{x}+1, \bar{y}, \bar{z}$. [b] $x, y, z-1$. [c] $x, y-1, z-1$. [d] $\bar{x}+1, \bar{y}, \bar{z}+1$. [e] $x, y, z+1$. [f] $\bar{x}+1, \bar{y}+1, \bar{z}$. [g] $\bar{x}, \bar{y}+1, \bar{z}$. [h] $x, y, z-2$. [i] $\bar{x}+1, \bar{y}+1, \bar{z}-1$. [j] $x-1, y, z-1$.

(10) Mueller, K. T.; Sun, B.; Chingas, G. C.; Zwanziger, J. W.; Terao, T.; Pines, A. *J. Magn. Reson.* **1990**, *86*, 470.
(11) Grandinetti, P. J.; Baltisberger, J. H.; Llor, A.; Lee, Y. K.; Werner, U.; Eastman, M. A.; Pines, A. *J. Magn. Reson.* **1993**, *A103*, 72.
(12) Ernst, R. R.; Bodenhausen, G.; Wokaun, A. *Principles of Nuclear Magnetic Resonance in One and Two Dimensions*; Oxford University Press: Oxford, 1989.

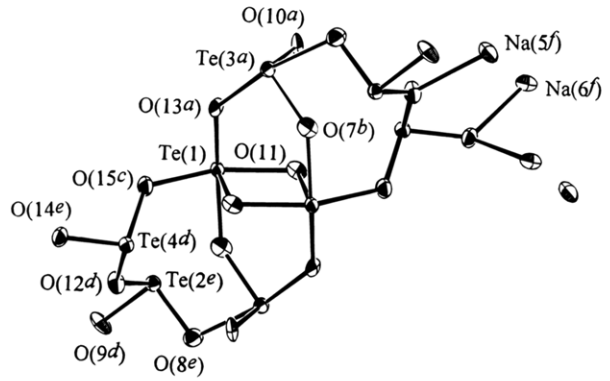

Figure 1. ORTEP drawing of $Na_2Te_4O_9$, showing numbering scheme and thermal ellipsoids (90% probability surfaces). Symmetry operations for superscripted numbers are as follows: [a] $x, y, z - 1$; [b] $\bar{x} + 1, \bar{y}, \bar{z}$; [c] $x, y - 1, z - 1$; [d] $x, y - 1, z$; [e] $\bar{x} + 1, \bar{y}, \bar{z}$; [f] $x, y - 1, z + 1$. Contacts of 2.4 Å or less are shown.

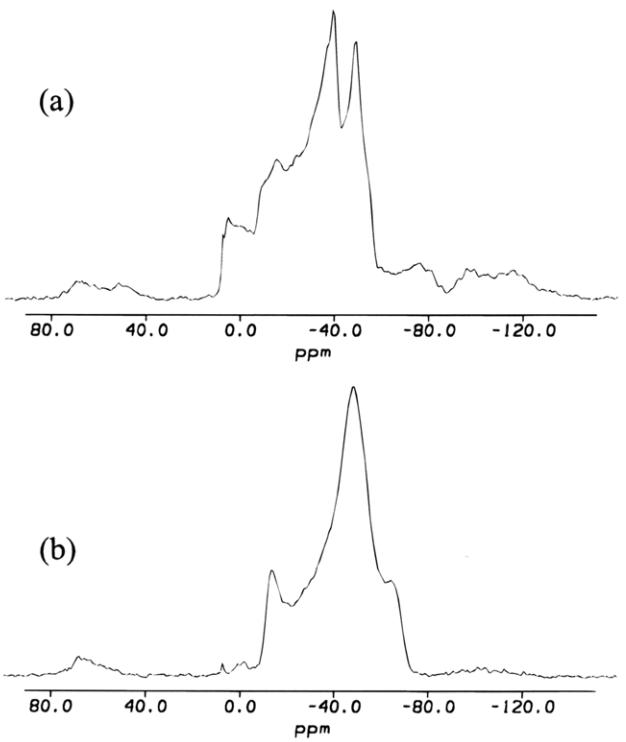

Figure 2. Sodium-23 NMR spectra of $Na_2Te_4O_9$ spinning at 7 kHz about an axis inclined at various angles with respect to the magnetic field. The field strength is 8.46 T. Shifts are relative to solid NaCl. (a) Rotor axis at 54.74°, the usual magic angle. (b) Rotor axis at 70.12°, the fourth-rank magic angle.

sional DAS spectrum of ^{23}Na in Na_2TeO_3, including the projections onto the isotropic shift dimension and the anisotropic plus isotropic shift dimension.

Discussion

Structure of the Crystalline Phases. There are two known crystalline forms of tellurium(IV) oxide: a colorless tetragonal form, α-TeO_2 (paratellurite),[6] and a yellowish orthorhombic form, β-TeO_2 (tellurite).[7] Both modifications are composed of four oxygen coordinated to one tellurium atom, with an average bond distance of 2.0 Å. These structures are often referred to as distorted trigonal bipyramids, when the equatorial site occupied by the lone pair of electrons is included in the structural description.[3,4,6,7] α-TeO_2 is a three-dimensional network of these TeO_4 units comprised of oxygen

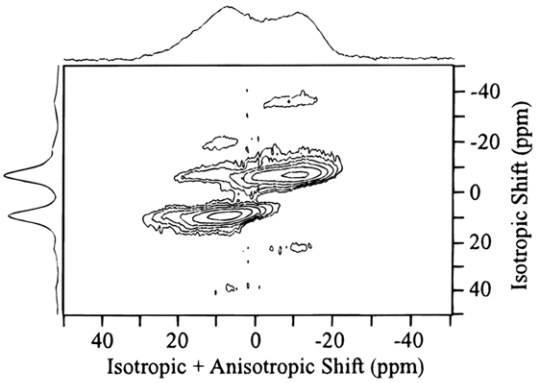

Figure 3. Sodium-23 DAS NMR spectra of Na_2TeO_3 at 8.46 T. Shifts are relative to solid NaCl. Shown at left is the projection onto the isotropic shift dimension of the DAS experiment.

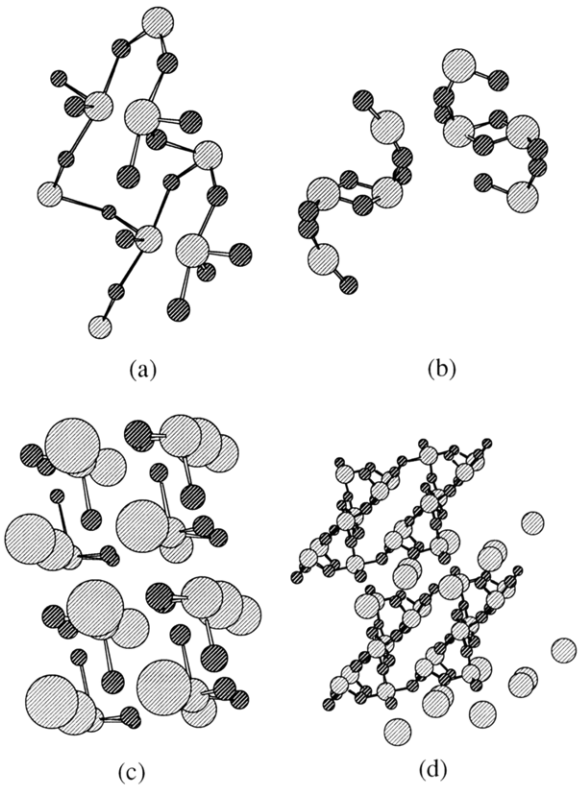

Figure 4. (a) Structure of α-TeO_2,[6] showing the three-dimensional network of corner-sharing trigonal bipyramids; light shaded circles are tellurium, dark are oxygen; (b) structure of β-TeO_2,[7] showing the edge-sharing units that make up the two-dimensional network (light circles are tellurium, dark are oxygen); (c) structure of Na_2TeO_3,[8] an ionic solid, consisting of TeO_3^{2-} pyramids (dark circles are oxygen, light are tellurium) coordinating Na^+ cations (large light circles); (d) structure of $Na_2Te_4O_9$, consisting of tellurite sheets interlayered with Na^+ ions; same shading as in structure (c).

atoms shared in an equatorial position to one TeO_4 unit and in an axial postion to another (Figure 4a). In β-TeO_2, pairs of TeO_4 groups are connected by a common edge to form Te_2O_6 units in infinite two-dimensional sheets (Figure 4b). In this form, as in the α phase, the oxygen are shared in a $Te-_{eq}O_{ax}-Te$ manner.

The compound Na_2TeO_3 has two sodium ions per unit cell, each octahedrally coordinated to the oxygen of TeO_3^{2-} trigonal pyramids (Figure 4c).[8] Thus, with the addition of 50 mol % Na_2O, the TeO_2 network is completely depolymerized. The cation environment in Na_2TeO_3 is different from any of the other alkali

tellurites: in Li_2TeO_3, Li^+ occupies tetrahedral sites[13] and in the potassium, rubidium, and cesium analogs there are three cations per unit cell.[14,15]

Crystalline $Na_2Te_4O_9$ has characteristics of both TeO_2 and Na_2TeO_3, specifically a combination of both bridging and nonbridging oxygen atoms (see Figures 1 and 4d). The structure is comprised of alternating layers of Na^+ cations and $Te_4O_9^{2-}$ polymeric sheets running parallel to the *c* axis. Na(5) is surrounded by six oxygen atoms in a pseudo-octahedral arrangement with one oxygen atom pushed out to a distance of 2.926 Å. This elongation makes the environment around the sodium ion more similar to a distorted trigonal bipyramid. Similarly, although Na(6) has five oxygen neighbors, the farthest being 2.713 Å away, its coordination roughly resembles a tetrahedron. Oxygen O(10) and O(14) are identifiable as nonbridging, with distances to Te(3) and Te(4) of 1.82 Å, respectively; no other tellurium atoms are within 2.5 Å of these oxygen. Both O(10) and O(14) coordinate to the sodium ions, but other bridging oxygen do as well. Three of the four tellurium, Te(2)–Te(4), show typical trigonal bipyramid bonding geometries, with two axial and two equatorial sites. One of the axial contacts of each of Te(2) and Te(3) are rather long, at 2.450 and 2.320 Å, respectively. The coordination of Te(1) is somewhat unusual. Two Te(1) atoms are connected via two O(11) atoms in an edge-sharing fashion, with a Te–Te distance of 3.165 Å, close to the 3.17 Å observed in β-TeO_2,[7] which also shows edge-sharing. In further analogy with β-TeO_2, each O(11) occupies an equatorial spot on one Te(1), and an axial spot on the other. The rest of the trigonal bipyramid is filled out by O(15) and O(13) in the other axial and equatorial locations, respectively. The presence of O(7) disrupts the similarity with β-TeO_2, however. It is 2.238 Å from Te(1), only slightly farther than the sum of covalent radii for oxygen and tellurium, and confers an odd 5-fold coordination to Te(1), which we might call TeO_{4+1}, in analogy with more common TeO_{3+1} structures.[3] Indeed, the bond valence (see below for details of calculations) for Te(1) is 4.3, as compared to a value of 4.0 for an ideal four-coordinate tellurium, which we take as further evidence for over-coordination of this site. It is interesting to note that a reasonable explanation for the coloration of β-TeO_2 is based on the short Te–Te distance.[7] As noted above, $Na_2Te_4O_9$ is colorless; it may be that the close contact of O(7) disrupts the electronic structure of the edge-sharing unit that gives color to β-TeO_2. We know of only two other compounds, β-$Li_2Te_2O_5$[16] and the mineral denningite[17] $(Mn,Ca,Zn)Te_2O_5$, that are reported to have edge-sharing Te_2O_6 units.

Sodium Cation Environments. We have characterized the sodium cation environments in both $Na_2Te_4O_9$ and Na_2TeO_3 with NMR experiments, as described above. The isotropic shifts in the DAS spectra yield a combination of the isotropic chemical shift and the quadrupole interaction parameters through

$$\delta_{iso} = \delta_{iso}^{(CS)} - \frac{3 \times 10^6}{40} \frac{[I(I+1) - 3/4]}{I^2(2I-1)^2} \frac{P_Q^2}{\nu_0^2} \quad (1)$$

where δ_{iso} is the isotropic shift in ppm, $\delta_{iso}^{(CS)}$ is the isotropic chemical shift, I is the nuclear spin ($I = 3/2$ for sodium-23) and ν_0 is the Larmor frequency in megahertz. The quadrupole product $P_Q = (e^2Qq/h) \times \sqrt{1 + \eta^2/3}$ contains the information about the quadrupole interaction. The field dependence in eq 1 permits separate determination of the chemical shift and the quadrupolar terms. We exploited this dependence to determine the P_Q and $\delta_{iso}^{(CS)}$ for sodium in Na_2TeO_3 by running DAS experiments at two fields. Adequate signal-to-noise was a problem in $Na_2Te_4O_9$ at the lower field, so we used a combination of DAS and line-shape analysis of the MAS and VAS spectra to obtain the parameters. Because of the second-order quadrupole interaction, the anisotropy of the sodium NMR signal varies, under fast spinning conditions, as

$$a_0 + a_2P_2(\cos\theta) + a_4P_4(\cos\theta) \quad (2)$$

where the a_i are constants, θ is the angle between the rotor axis and the magnetic field, and P_2 and P_4 are Legendre polynomials. The usual magic angle, $\theta_m^{(2)} = 54.74°$, is a zero of P_2 but not of P_4. The resulting line shape, shown for $Na_2Te_4O_9$ in Figure 2a, is rather complicated but can be used to determine η from the spacing between the singularities. The angle $\theta_m^{(4)} = 70.12°$, where P_4 goes to zero, is also helpful. It yields simpler spectra (Figure 2b), from which e^2Qq/h and $\delta_{iso}^{(CS)}$ can be determined. We supplemented these spectra with others at different angles, to confirm our parameter assignments. Line shapes for different parameters and rotor axis angles were computed using the algorithm of Alderman et al.,[18] using formulas for the anisotropic frequency of the second-order quadrupole interaction developed from the perturbation theory of ref 19. Optimization of the parameters was accom-

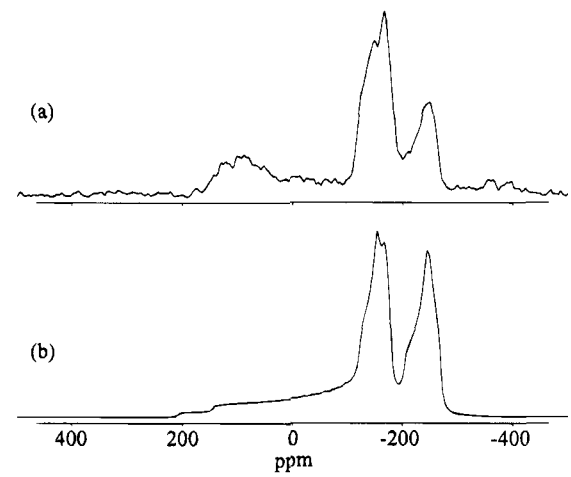

Figure 5. (a) Sodium-23 NMR spectrum of $Na_2Te_4O_9$ at 4.7 T, with rotor axis inclined at 79.19° with respect to the magnetic field. (b) Simulated line shape for this configuration, with the parameters for the two sodium sites given in Table 5.

(13) Folger, F. *Z. Anorg. Allg. Chem.* **1975**, *411*, 103.
(14) Andersen, L.; Langer, V.; Strömberg, A.; Strömberg, D. *Acta Crystallogr.* **1989**, *B45*, 344.
(15) Thümmel, H.-J.; Hoppe, R. *Z. Naturforsch.* **1974**, *29b*, 28.
(16) Cachaut-Herreillat, D.; Norbert, A.; Maurin, M.; Phillipot, E. *J. Solid State Chem.* **1981**, *37*, 352.
(17) Wells, A. F. *Structural Inorganic Chemistry*; Oxford University Press: Oxford, 1984.
(18) Alderman, D. W.; Solum, M. S.; Grant, D. M. *J. Chem. Phys.* **1986**, *84*, 3717.
(19) Goldman, M.; Grandinetti, P. J.; Llor, A.; Olejniczak, Z.; Sachleben, J. R.; Zwanziger, J. W. *J. Chem. Phys.* **1992**, *97*, 8947.

Table 5. Measured and Modeled NMR Parameters in $Na_2Te_4O_9$ and Na_2TeO_3[a]

compound	site	e^2Qq/h, MHz	e^2Qq/h, MHz (model)	σ_{iso}, ppm	σ_{iso}, ppm (model)	η
$Na_2Te_4O_9$	Na(5)	4.4 ± 0.2	4.18	−3 ± 5	−11.8	0.08 ± 0.05
	Na(6)	3.6 ± 0.2	3.61	5 ± 10	−5.2	0.12 ± 0.05
Na_2TeO_3	Na(1)	1.84 ± 0.05	1.96	5.8 ± 0.5	3.1	0.8 ± 0.1
	Na(2)	1.36 ± 0.05	1.22	17.0 ± 0.5	4.8	0.9 ± 0.1

[a] The chemical shifts are modeled with eq 3 and the correlation of Koller et al.,[21] and the quadrupole interaction values are based on the point-charge model and the correlation of eq 7. Shifts are relative to solid NaCl. The site numbers for Na_2TeO_3 are taken from ref 8.

plished by a combination of graphical means and a downhill-simplex method.[20] This procedure was most effective for spectra obtained in the lower field, 4.7 T, due to the increased dispersion. A result is shown in Figure 5, for the NMR spectrum of $Na_2Te_4O_9$ at 4.7 T, spinning rapidly about an axis inclined at 79.19° with respect to the magnetic field. The parameters for the sodium sites in $Na_2Te_4O_9$ and Na_2TeO_3 are listed in Table 5.

The various NMR parameters for each site contain information about the types of interactions to which the ions are subject, and through use of various models of these interactions, general correlations can be obtained. This approach for sodium has been recently described,[21,22] and we follow here the work of Koller et al.[21] The chemical shifts are modeled through the parameter A, where

$$A = \sum_i W_i/r_i^3 \tag{3}$$

Here r_i is the distance from the sodium of interest to the ith oxygen atom, which has valency W_i. The valency is computed from the empirical parameters of Brown and Altermatt[23] (see also refs 24 and 25). Koller et al. found a reasonable correlation between A and the chemical shift for sodium in a variety of oxide materials, mainly silicates. Their correlation takes the form $\delta_{iso}^{(CS)} = -133.6A + 107.6$. Physically this form suggests that, distances being equal, sodium sites coordinated by oxygen with lower valency (W) will be shifted downfield. The distance dependence is strong, however, so in fact small changes in the geometry of the coordination sphere make a considerable difference in the actual shift. A comparison of our experimental shifts with this model is presented in Table 5, where it is seen that the two are in qualitative agreement. We were not able to establish a better correlation for the particular compounds studied here.

We were able to find an improved correlation for the quadrupole interaction, however. Again, as in ref 21, the quadrupole interaction is computed from a point-charge model, with the charge localized on the neighboring oxygen atoms. The magnitude of charge, q, was computed from

$$q = -2 + \sum_i f_i \tag{4}$$

where f_i is the covalency obtained from the empirical bond strength parameters of Brown and Shannon.[24] We found in Na_2TeO_3, in which all oxygen are nonbridging, typical effective charges of $-0.9e$, and in $Na_2Te_4O_9$, which has more covalent character, $-0.7e$. From these effective charges and the structure, we computed electric field gradients at the sodium sites. Diagonalizing the resulting tensor yields the principal elements of the electric field gradient. The strength of the quadrupole interaction was then obtained from

$$e^2Qq/h = (eQ)(eq)(1 - \gamma_\infty)/h \tag{5}$$

where Q is the quadrupole moment of sodium-23 (0.10×10^{-24} cm^2 [26]), $eq = V_{zz}$ is the largest (in magnitude) component of the electric field gradient, γ_∞ is the Sternheimer factor (for ^{23}Na, $\gamma_\infty = -4.1$, refs 21 and 27), and h is Planck's constant. The asymmetry η of the quadrupole interaction was also computed, from

$$\eta = (V_{yy} - V_{xx})/V_{zz} \tag{6}$$

Using this approach Koller et al. obtained a good correlation between calculated and measured values for e^2Qq/h but not for η. We observe similar behavior in this data set. We found that the correlation they derived uniformly underestimates e^2Qq/h in these materials, probably because the empirical parameters used to calculate the effective charge q were not optimized for tellurium compounds. Using our data we have obtained the following correlation for e^2Qq/h:

$$e^2Qq/h = 1.77(e^2Qq/h)_{PC} + 0.14 \tag{7}$$

where $(e^2Qq/h)_{PC}$ is the value computed from the point-charge model. For this fit $R^2 = 0.98$. A comparison of this model and the experimental values is given in Table 5. The agreement for e^2Qq/h is seen to be good for all sites measured in this study. In Na_2TeO_3, for which both sodium sites are octahedrally coordinated, we observe relatively small values of e^2Qq/h. Within the point-charge model this can be understood as the cancellation of the field gradients due to the symmetry of the oxygen coordination shell surrounding each sodium. The e^2Qq/h values in $Na_2Te_4O_9$ are considerably larger, due to the lower symmetry of the coordination in this compound. The value for Na(6) is the smaller of the two. This is surprising at first glance, because this site is coordinated by five oxygen, as

(20) Press, W. H.; Flannery, B. P.; Teukolsky, S. A.; Vetterling, W. T. *Numerical Recipes in C*; Cambridge University Press: Cambridge, 1988.
(21) Koller, H.; Engelhardt, G.; Kentgens, A. P. M.; Sauer, J. *J. Phys. Chem.* **1994**, *98*, 1544.
(22) Xue, X.; Stebbins, J. F. *Phys. Chem. Miner.* **1993**, *20*, 297.
(23) Brown, I. D.; Altermatt, D. *Acta Crystallogr.* **1985**, *B41*, 244.
(24) Brown, I. D.; Shannon, R. D. *Acta Crystallogr.* **1973**, *A29*, 266.
(25) Brese, N. E.; O'Keeffe, M. *Acta Crystallogr.* **1991**, *B47*, 192.
(26) Anderson, H. L., Ed. *A Physicist's Desk Reference: Physics Vade Mecum*, 2nd ed.; American Institute of Physics: New York, 1989.
(27) Slichter, C. P. *Principles of Magnetic Resonance*, 3rd ed.; Springer: New York, 1989.
(28) Hamilton, W. C. *Acta Crystallogr.* **1959**, *12*, 609.
(29) Giacovazzo, C. The diffraction of X-rays by crystals. In Giacovazzo, C., Ed.; *Fundamentals of Cystallography*; International Union of Crystallography, Oxford Science Publications: New York, 1992.

opposed to six for Na(5). However, one of the five is considerably removed from Na(6) and contributes very little to the field gradient, owing to the $1/r^3$ distance dependence. The remaining four oxygens form a distorted tetrahedron, which is of sufficient symmetry to keep the quadrupole interaction relatively small. One of the oxygen coordinating Na(5) is also distant, and the remaining five oxygen present a trigonal bipyramid structure, which explains the large value of e^2Qq/h observed for this site. Finally, we note that the asymmetry η computed for each site within the point-charge model did not correspond well with the observed values; Koller et al. reached a similar conclusion.[21]

Conclusions

We have succeeded in solving the crystal structure of $Na_2Te_4O_9$, which we believe will be an important result for understanding the microstructure and glass-forming characteristics of the $(Na_2O)_x(TeO_2)_{1-x}$ system. The structure consists of tellurium oxide sheets separated by sodium cations; within each sheet there are edge-sharing Te_2O_6 fragments, as well as corner-bridged tellurium with nonbridging oxygen. We have also investigated the sodium cation binding in $Na_2Te_4O_9$ and Na_2TeO_3 and found that simple models of the chemical shift and quadrupole interaction provide good agreement with experiment. This result provides a basis for interpreting NMR results on the glasses in this system, work that is currently underway in our laboratory.

Acknowledgment. We thank R. E. Youngman for assistance with the NMR experiments and Prof. M. D. Hollingsworth for helpful discussions. S.L.T. gratefully acknowledges financial support from the Department of Education National Needs Program. This research was supported by the National Science Foundation under Grant No. DMR-9115787.

Supplementary Material Available: List of thermal parameters for $Na_2Te_4O_9$ (1 page); list of observed and calculated structure factors for $Na_2Te_4O_9$ (6 pages). Ordering information is given on any current masthead page.